Gli impatti dei cambiamenti climatici sulle acque sotterranee e superficiali

Venerdì 27 ottobre 2023
Firenze, Piazza Duomo 10
Palazzo Sacrati - Sala delle Esposizioni

Sistema Nazionale per la Protezione dell'Ambiente

ARPAT
Agenzia regionale per la protezione ambientale della Toscana

REGIONE TOSCANA

UNIVERSITÀ DEGLI STUDI FIRENZE

DST DIPARTIMENTO DI SCIENZE DELLA TERRA

ECCELLENZA 2023-27

" Cambiamenti climatici e dispersione di contaminanti: il caso del fiume Paglia".

Pilario Costagliola

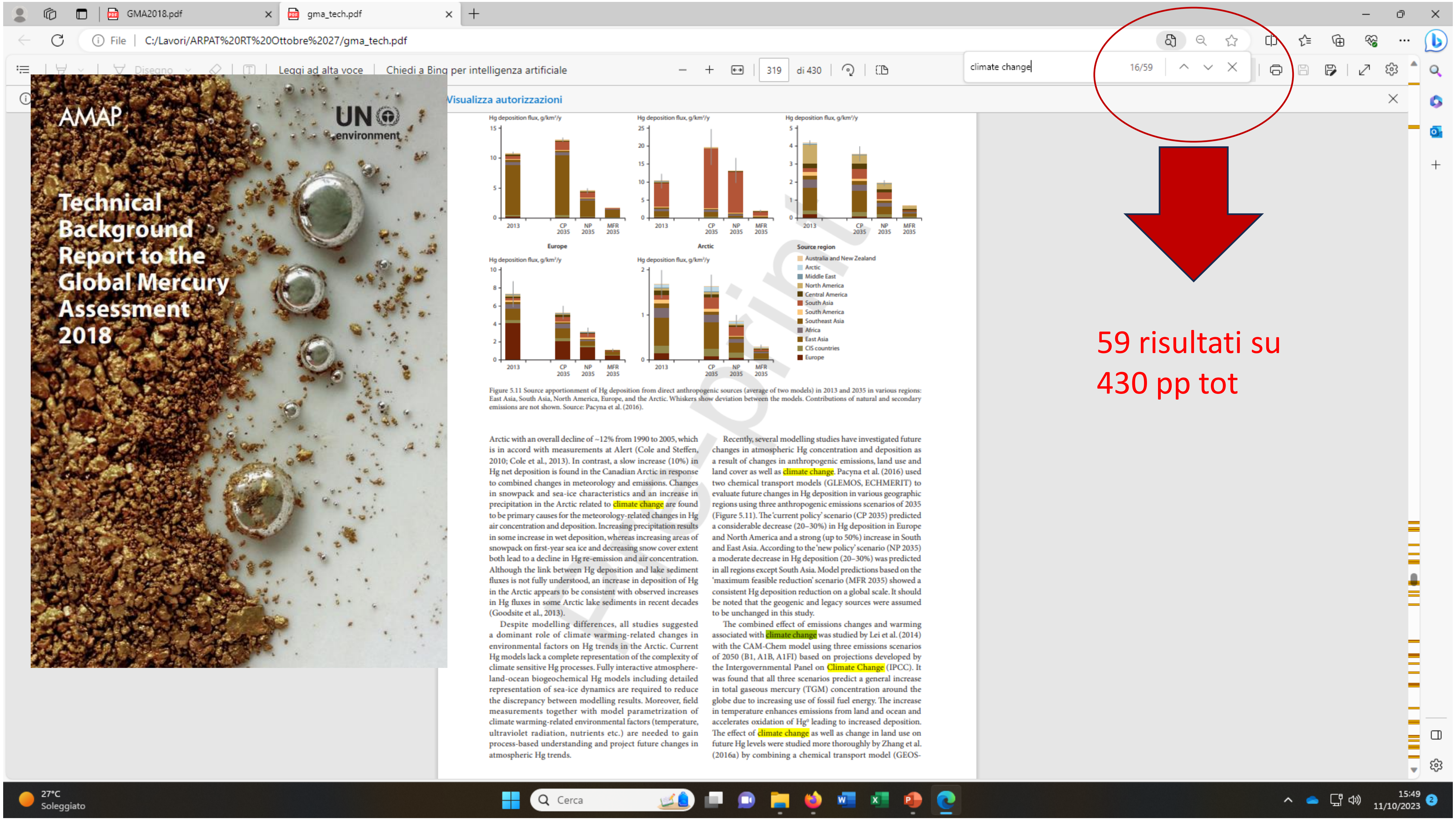

Figure 5.11 Source apportionment of Hg deposition from direct anthropogenic sources (average of two models) in 2013 and 2035 in various regions: East Asia, South Asia, North America, Europe, and the Arctic. Whiskers show deviation between the models. Contributions of natural and secondary emissions are not shown. Source: Pacyna et al. (2016).

Arctic with an overall decline of ~12% from 1990 to 2005, which is in accord with measurements at Alert (Cole and Steffen, 2010; Cole et al., 2013). In contrast, a slow increase (10%) in Hg net deposition is found in the Canadian Arctic in response to combined changes in meteorology and emissions. Changes in snowpack and sea-ice characteristics and an increase in precipitation in the Arctic related to climate change are found to be primary causes for the meteorology-related changes in Hg air concentration and deposition. Increasing precipitation results in some increase in wet deposition, whereas increasing areas of snowpack on first-year sea ice and decreasing snow cover extent both lead to a decline in Hg re-emission and air concentration. Although the link between Hg deposition and lake sediment fluxes is not fully understood, an increase in deposition of Hg in the Arctic appears to be consistent with observed increases in Hg fluxes in some Arctic lake sediments in recent decades (Goodsite et al., 2013).

Despite modelling differences, all studies suggested a dominant role of climate warming-related changes in environmental factors on Hg trends in the Arctic. Current Hg models lack a complete representation of the complexity of climate sensitive Hg processes. Fully interactive atmosphere-land-ocean biogeochemical Hg models including detailed representation of sea-ice dynamics are required to reduce the discrepancy between modelling results. Moreover, field measurements together with model parametrization of climate warming-related environmental factors (temperature, ultraviolet radiation, nutrients etc.) are needed to gain process-based understanding and project future changes in atmospheric Hg trends.

Recently, several modelling studies have investigated future changes in atmospheric Hg concentration and deposition as a result of changes in anthropogenic emissions, land use and land cover as well as climate change. Pacyna et al. (2016) used two chemical transport models (GLEMOS, ECHMERIT) to evaluate future changes in Hg deposition in various geographic regions using three anthropogenic emissions scenarios of 2035 (Figure 5.11). The 'current policy' scenario (CP 2035) predicted a considerable decrease (20–30%) in Hg deposition in Europe and North America and a strong (up to 50%) increase in South and East Asia. According to the 'new policy' scenario (NP 2035) a moderate decrease in Hg deposition (20–30%) was predicted in all regions except South Asia. Model predictions based on the 'maximum feasible reduction' scenario (MFR 2035) showed a consistent Hg deposition reduction on a global scale. It should be noted that the geogenic and legacy sources were assumed to be unchanged in this study.

The combined effect of emissions changes and warming associated with climate change was studied by Lei et al. (2014) with the CAM-Chem model using three emissions scenarios of 2050 (B1, A1B, A1FI) based on projections developed by the Intergovernmental Panel on Climate Change (IPCC). It was found that all three scenarios predict a general increase in total gaseous mercury (TGM) concentration around the globe due to increasing use of fossil fuel energy. The increase in temperature enhances emissions from land and ocean and accelerates oxidation of Hg^0 leading to increased deposition. The effect of climate change as well as change in land use on future Hg levels were studied more thoroughly by Zhang et al. (2016a) by combining a chemical transport model (GEOS-

59 risultati su 430 pp tot

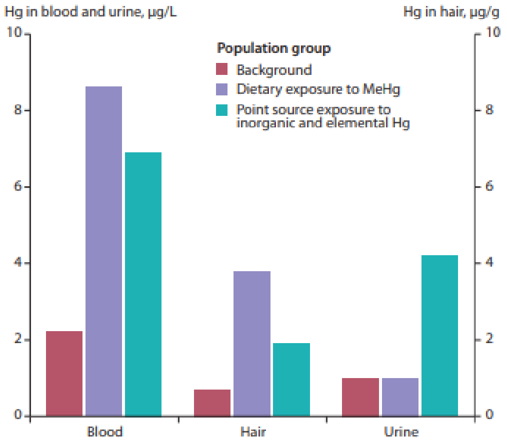

Figure 9.6 Median blood, hair, and urine Hg levels across different population groups following a systematic review of relevant cross-sectional studies.

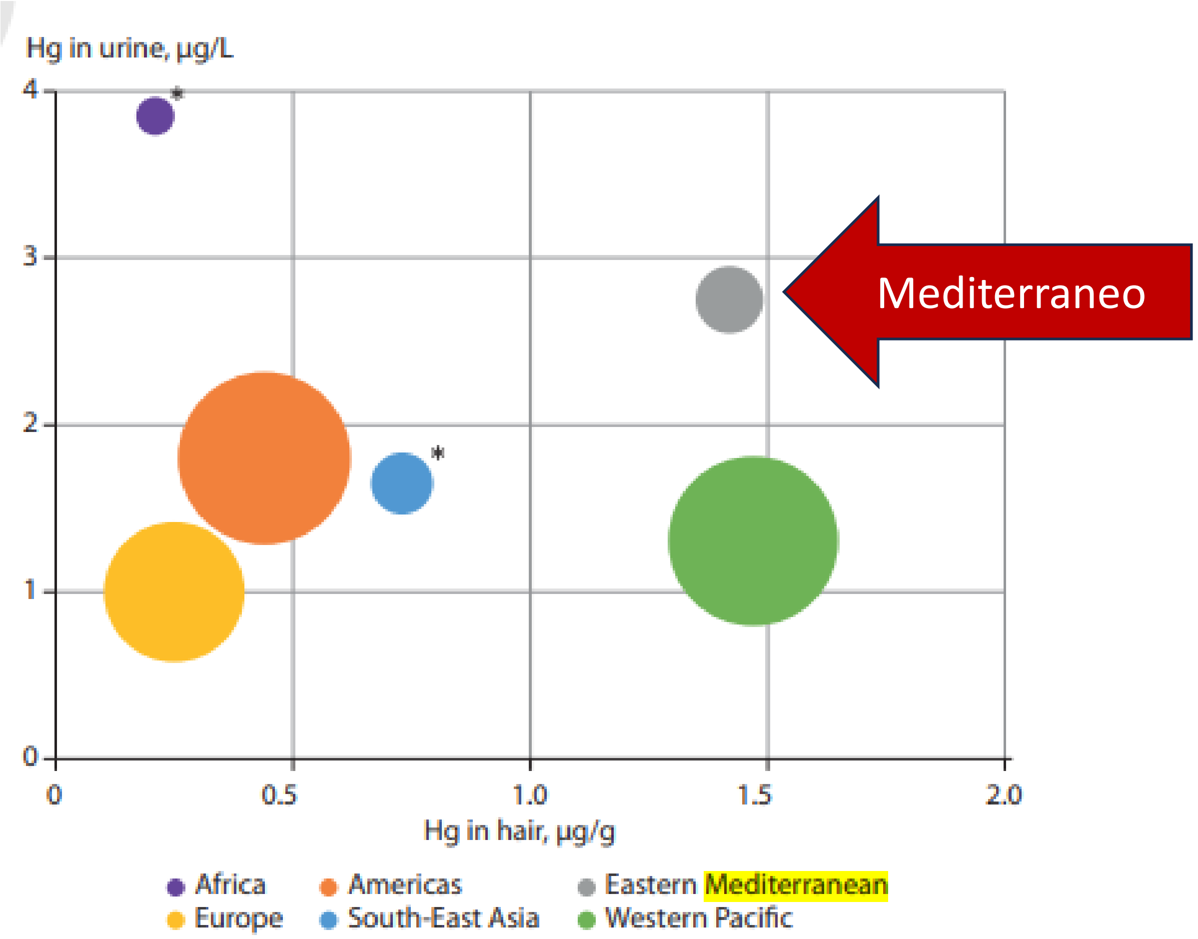

Figure 9.5 Bubble plot of hair and urine Hg levels from cross-sectional studies on background populations according to WHO geographic regions. The size of the bubble reflects the sample size. The asterisk indicates that urinary Hg levels from background populations in Africa and South-East Asia were not available, and thus urinary Hg levels from all populations within these regions was used.

- Molte cause
- Il cambiamento climatico porterà ad una complicazione del sistema
- Quello che abbiamo imparato potrebbe non servire più
- Abbiamo bisogno di più dati

Fiume Paglia

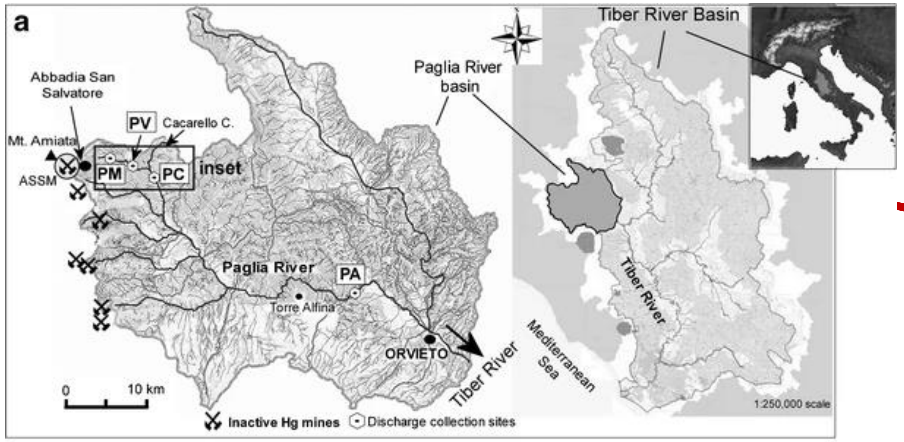

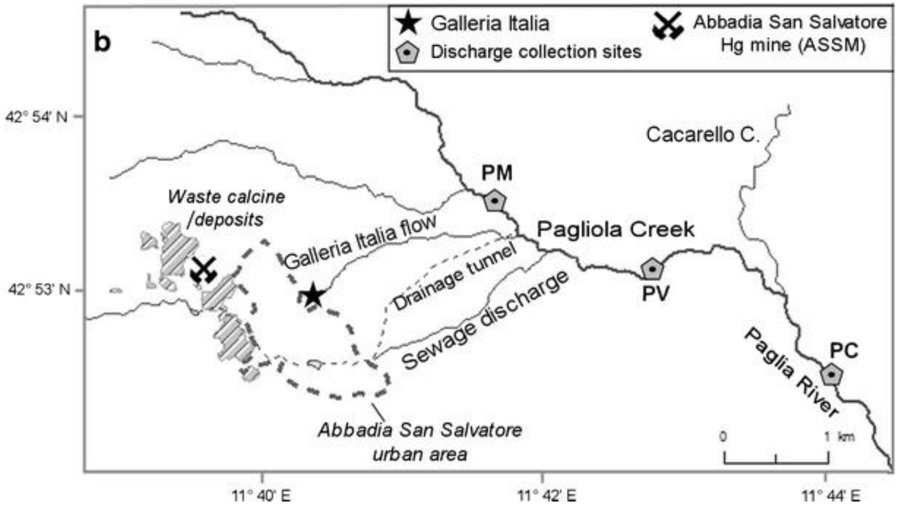

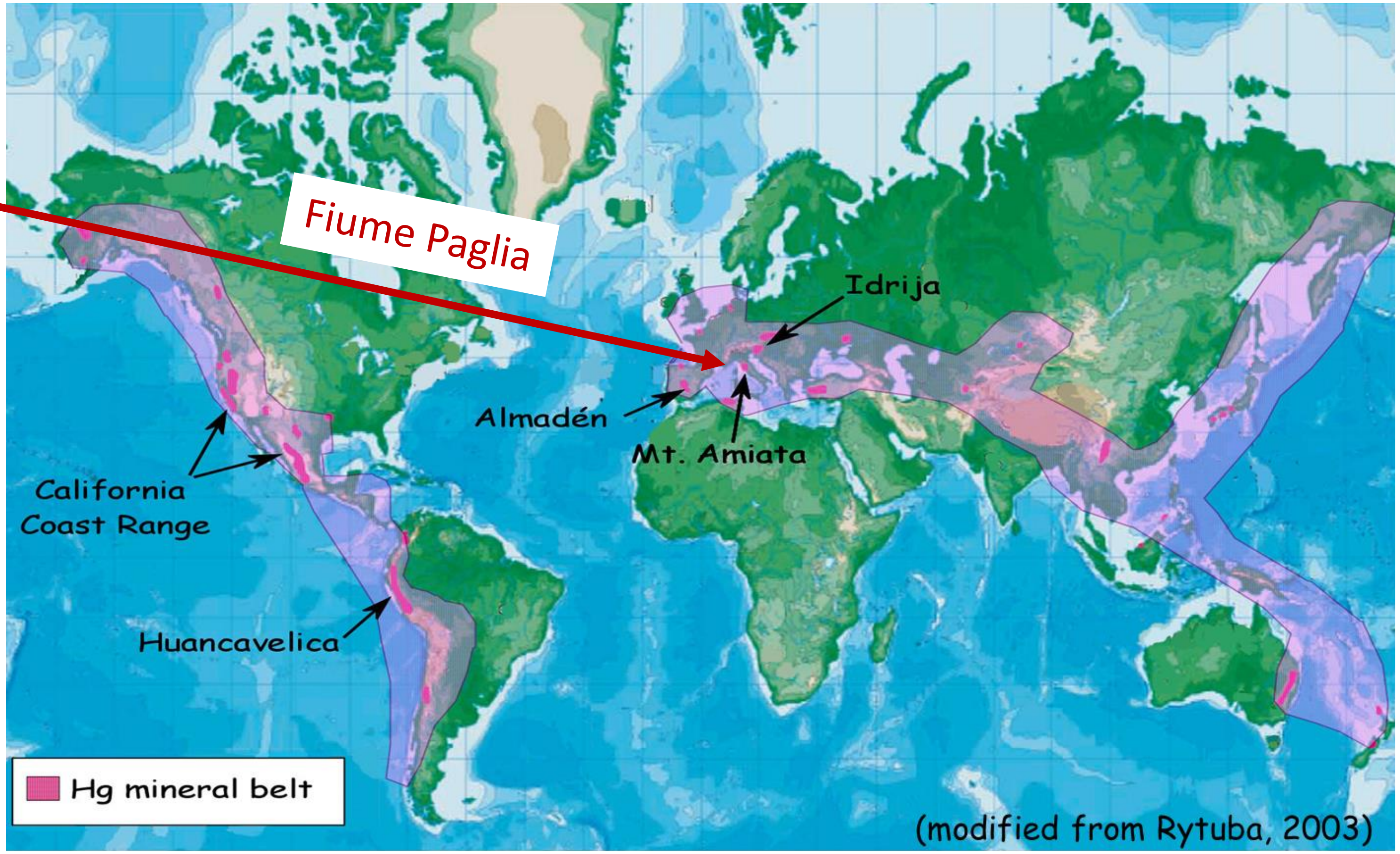

Paglia e Monte Amiata (Abbadia San Salvatore)

Studio DST - Arpa Toscana Umbria lazio

Fiume Paglia

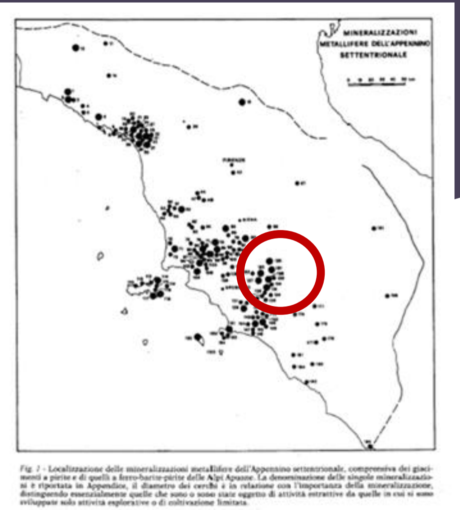

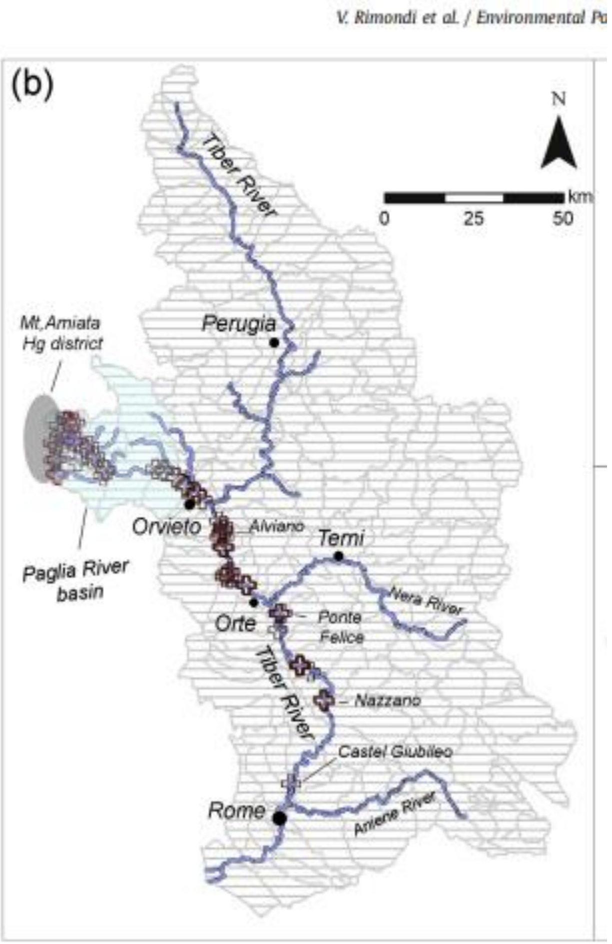

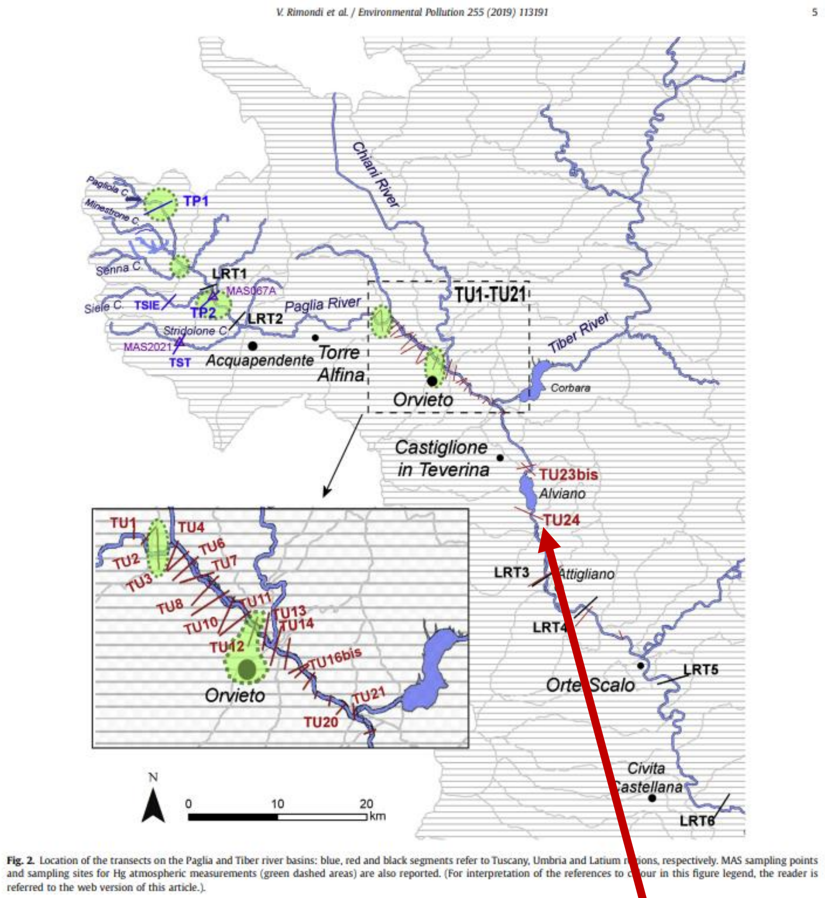

Bacino di Alviano

Cambiamenti climatici e Hg

- Trasporto Hg eventi di piena
- Aumento temperature e produzione di MeHg
- Effetto incendi

Trasporto Hg lungo il sistema Paglia Tevere: particolato

5582 Environ Sci Pollut Res (2014) 21:5575–5585

Fig. 6 Total, particulate and dissolved Hg mass loads ($M\text{-}Hg_T$, $M\text{-}Hg_P$, $M\text{-}Hg_D$) for the PRB in March and September 2011 and March 2012. Refer to the *left y*-axis for values of $M\text{-}Hg_T$ and $M\text{-}Hg_P$, to the *right y*-axis for $M\text{-}Hg_D$. For a graphical purpose, Hg mass loads at PM are set equal to zero in September 2011. Negative distances are upstream from the ASSM

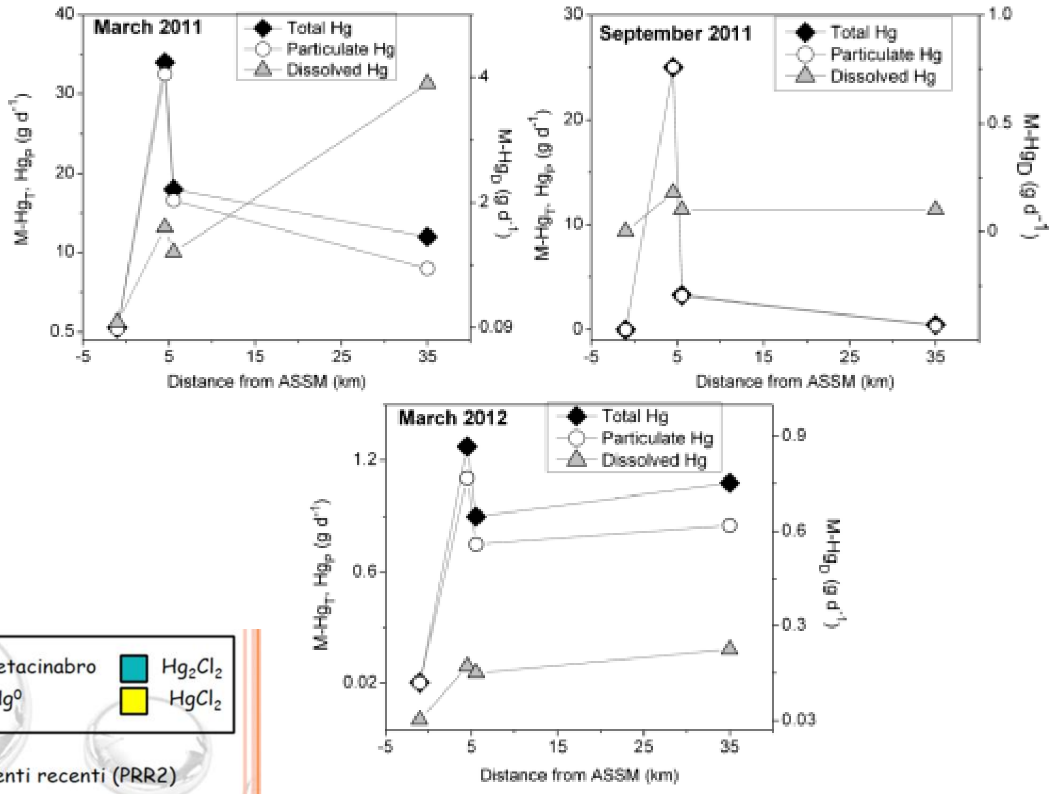

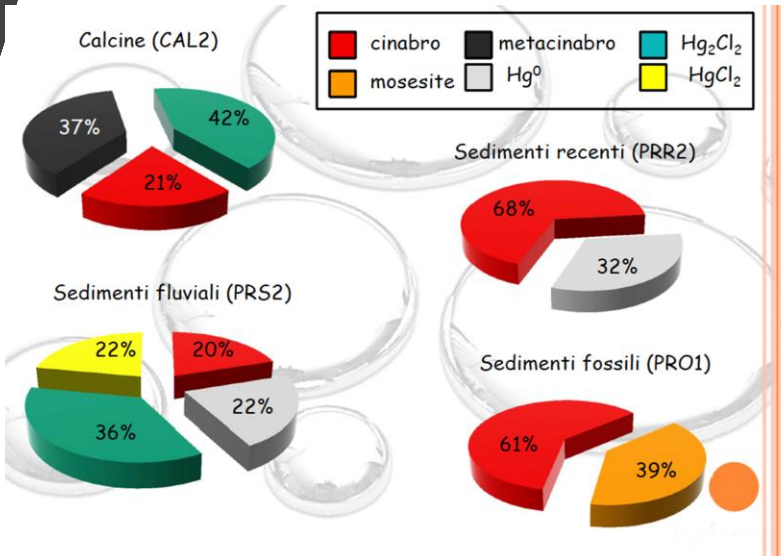

Evoluzione morfologica pianura alluvionale del Paglia (DST ArpaT)

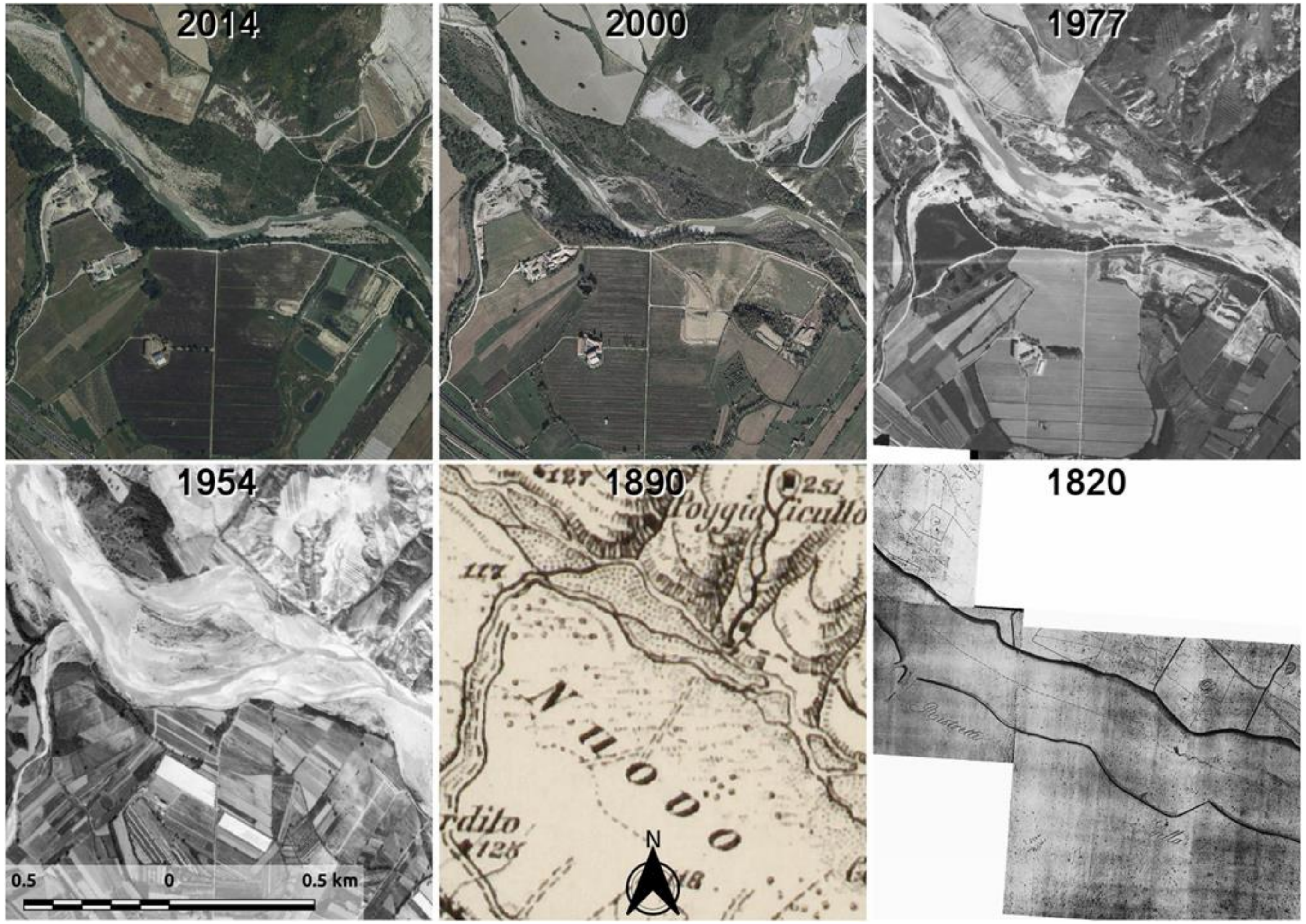

Inizio coltivazione

Paglia Allerona

Dimensioni del corridoio: ARPAT UNIFI

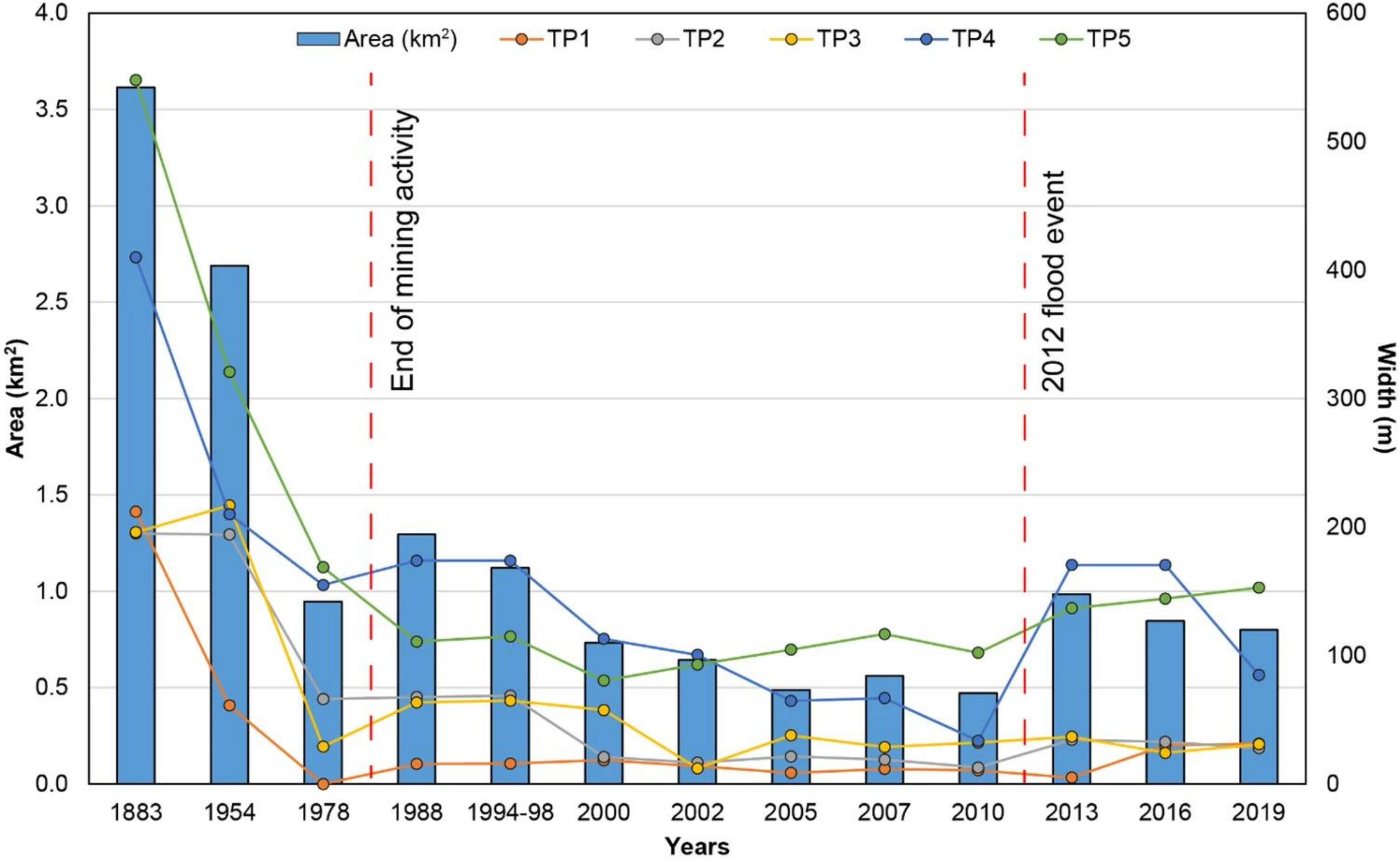

Il "Corridoio"

Collaborazione DST-ARPAT

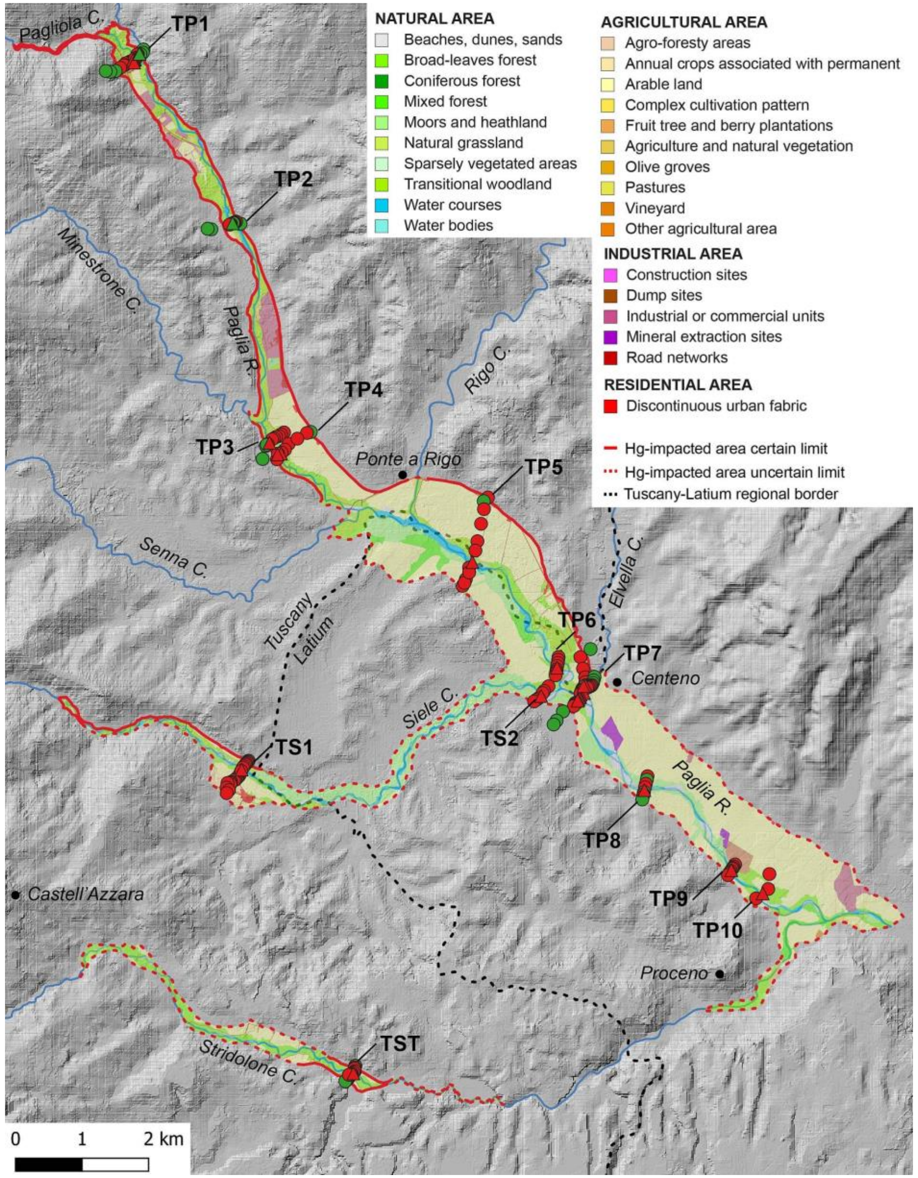

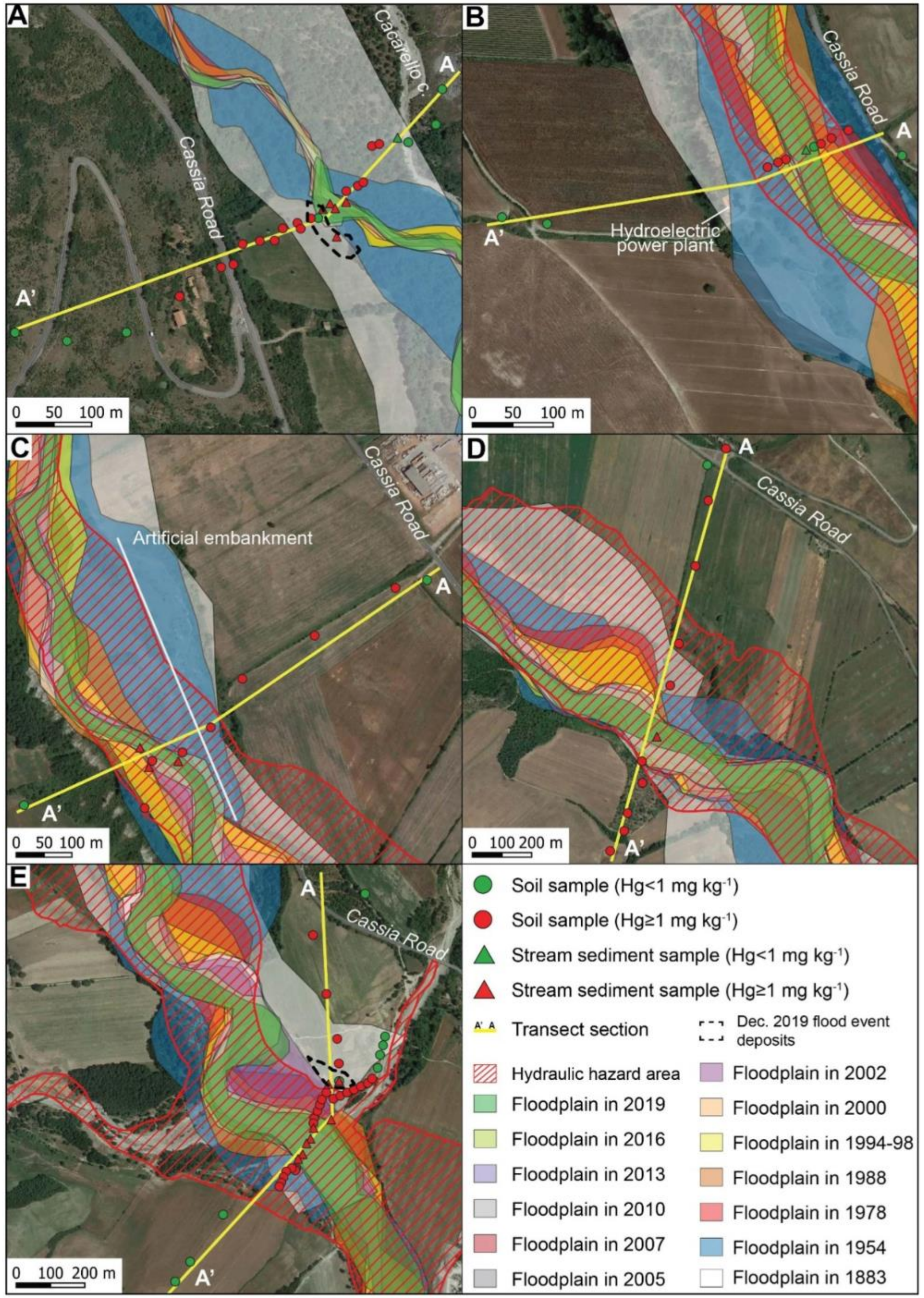

Corridoio e rischio idraulico

Effetto eventi piena nel corridoio

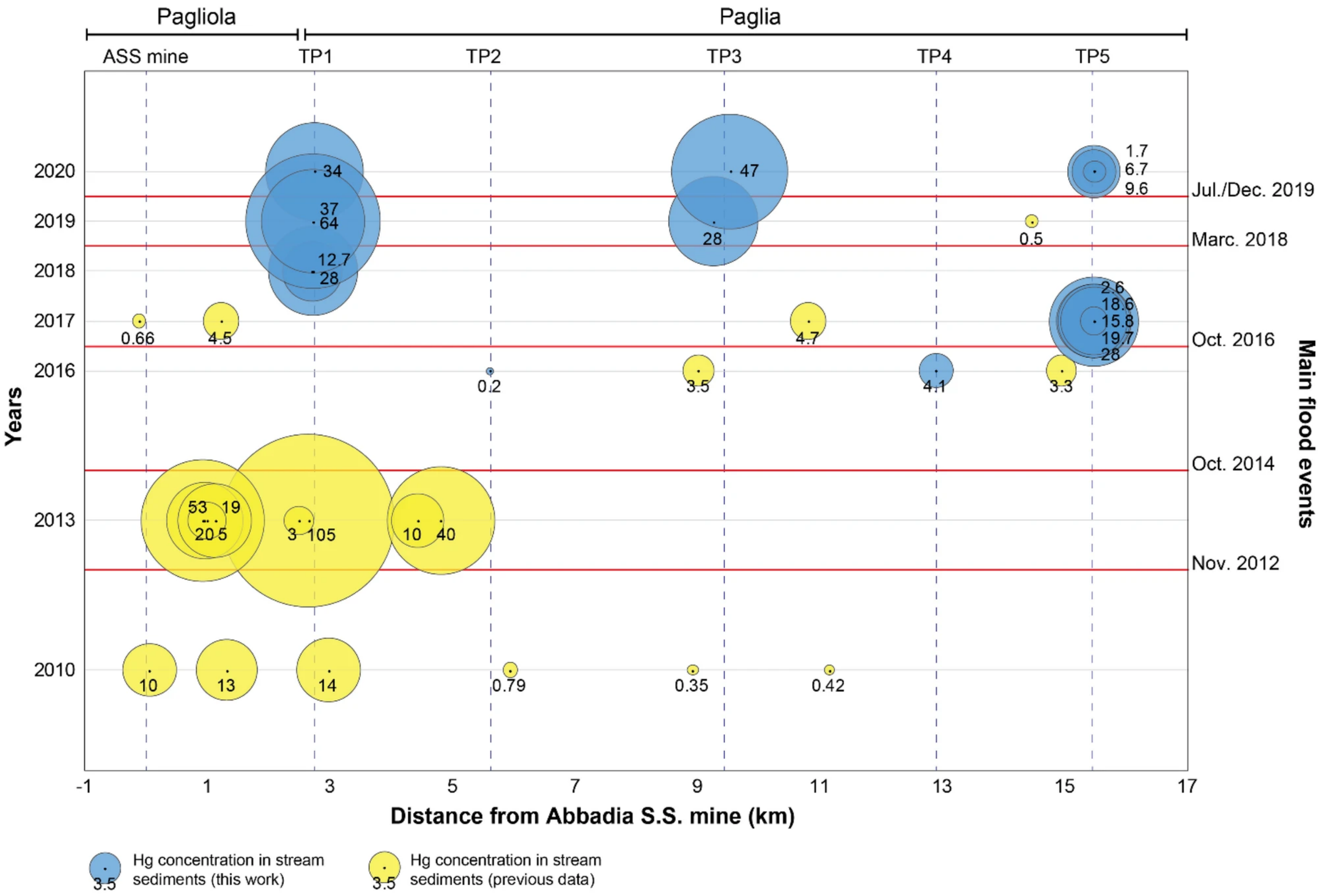

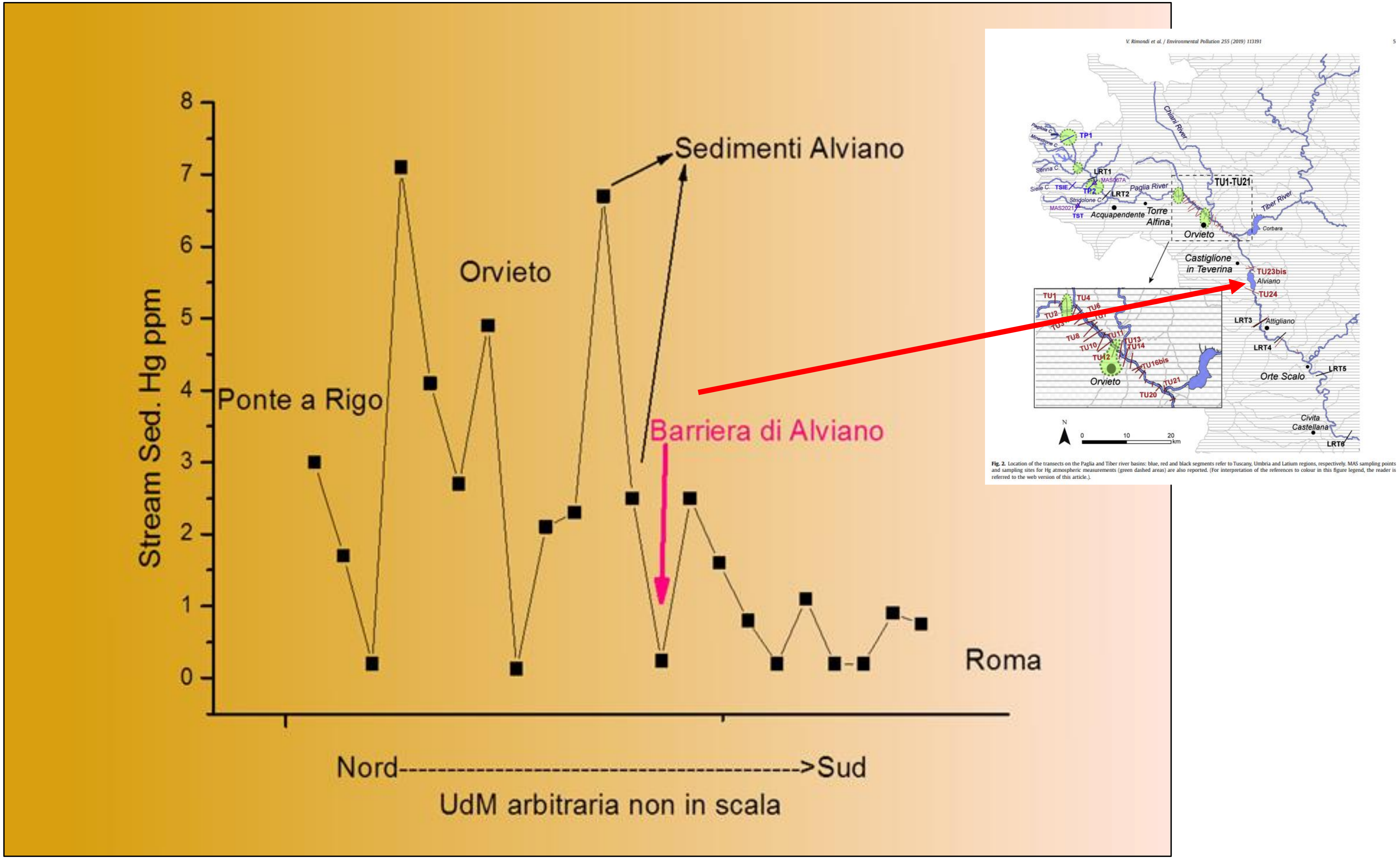
Stream Sed. Hg ppm
0
1
2
3
4
5
6
7
8
Ponte a Rigo
Orvieto
Sedimenti Alviano
Barriera di Alviano
Roma
Nord-->Sud
UdM arbitraria non in scala
V. Rimondi et al. / Environmental Pollution 255 (2019) 113191
5
Chiani River
Paglia River
Tiber River
TP1
TP2
TSIE
TST
LRT1
LRT2
LRT3
LRT4
LRT5
LRT6
MAS2021
TU1-TU21
Acquapendente
Torre Alfina
Orvieto
Corbara
Castiglione in Teverina
TU23bis
Alviano
TU24
Attigliano
Orte Scalo
Civita Castellana
N
0
10
20
km
Fig. 2. Location of the transects on the Paglia and Tiber river basins: blue, red and black segments refer to Tuscany, Umbria and Latium regions, respectively. MAS sampling points and sampling sites for Hg atmospheric measurements (green dashed areas) are also reported. (For interpretation of the references to colour in this figure legend, the reader is referred to the web version of this article.).


Osservatorio Geofisico di Modena:
temperature massime giornaliere del 2022
Confronto con Estate 2003
Temp.Max 2022
tmax 2003
Temperatura (°C)
40
35
30
25
20

Estate 2022
lago Alviano
Analisi ARPAT
MeHg

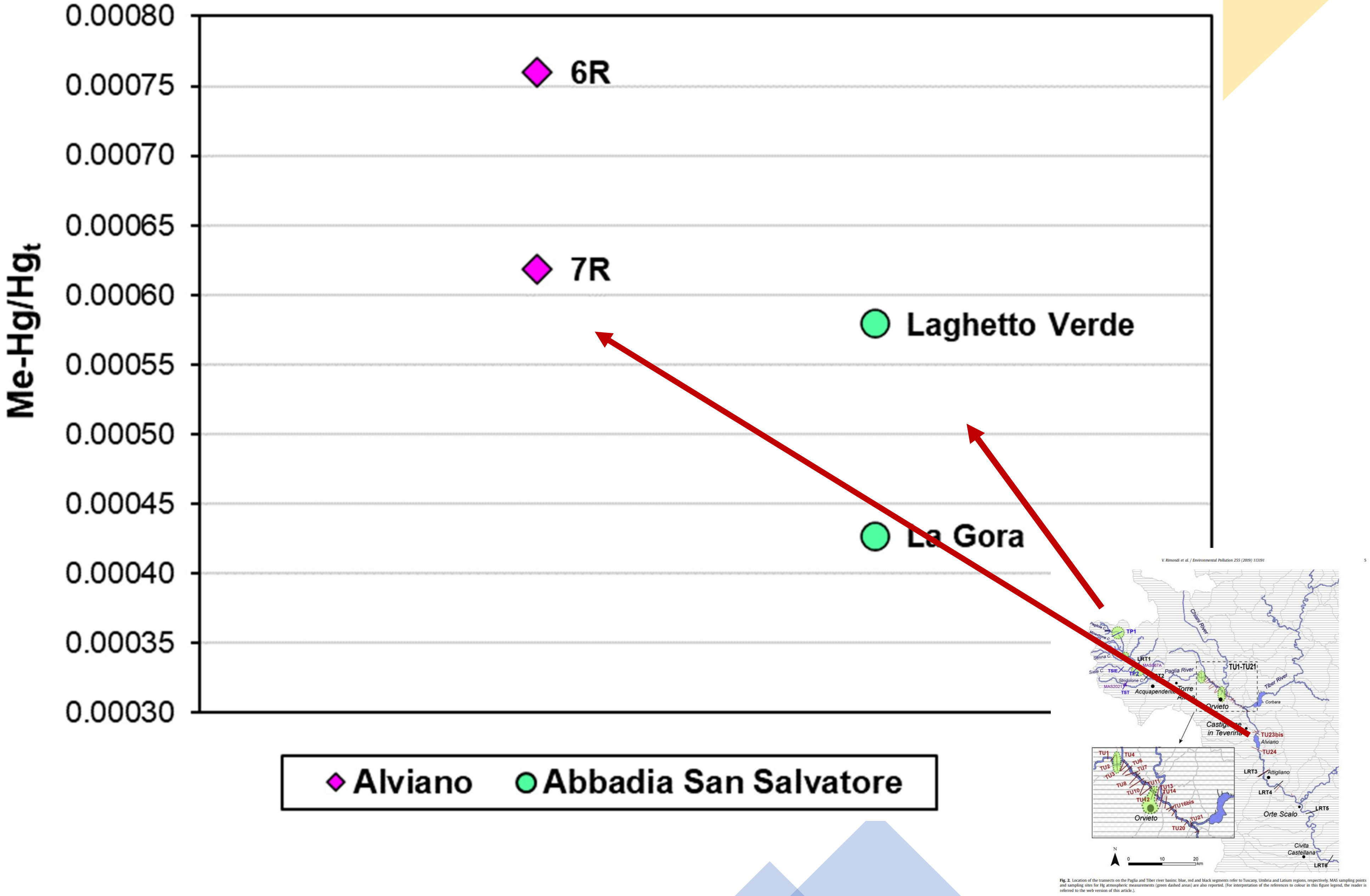

Incendi

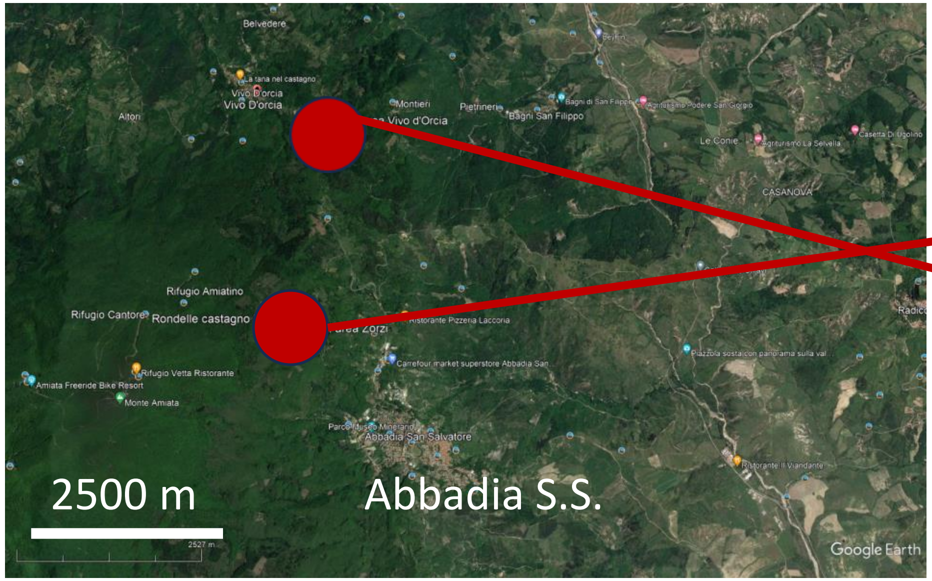
2500 m
Abbadia S.S.
Google Earth

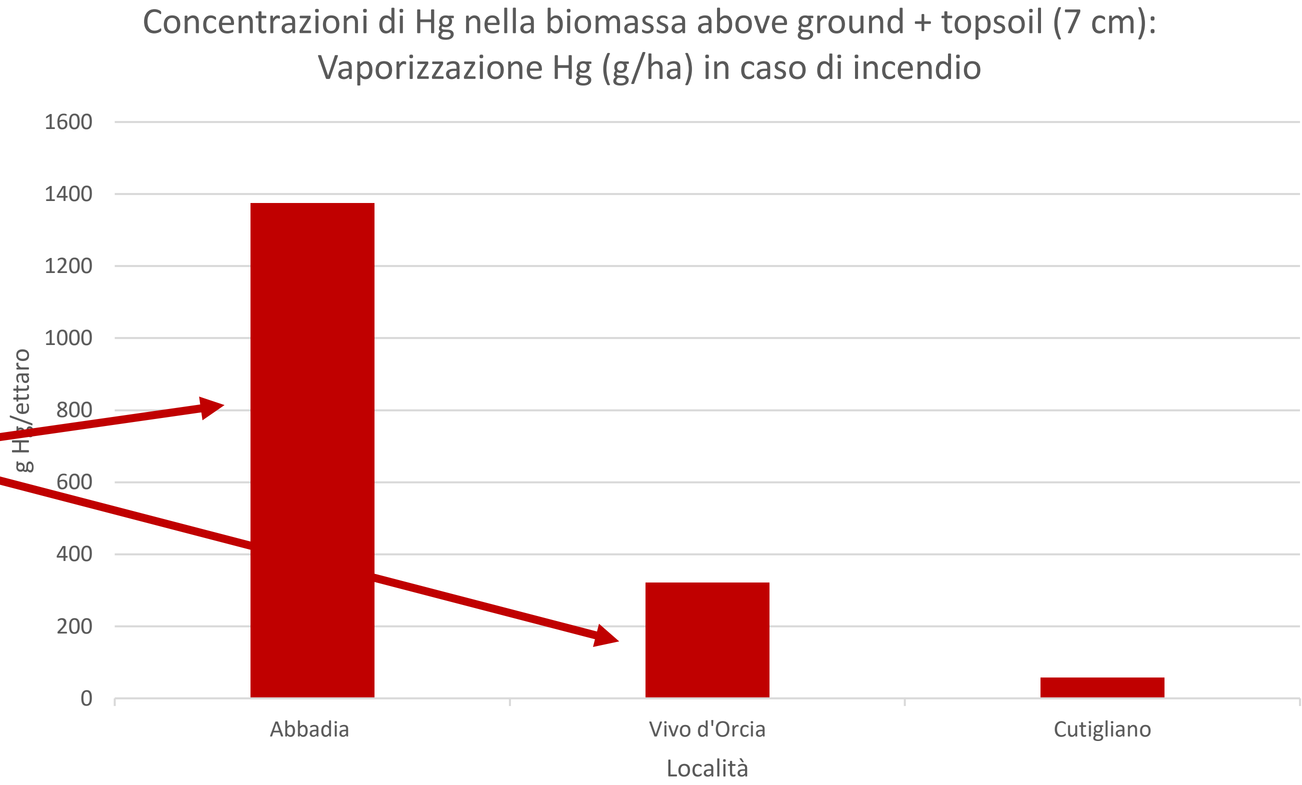
Concentrazioni di Hg nella biomassa above ground + topsoil (7 cm):
Vaporizzazione Hg (g/ha) in caso di incendio
1600
1400
1200
1000
800
600
400
200
0
g Hg/ettaro
Abbadia
Vivo d'Orcia
Cutigliano
Località

Possibili interventi

1) Monitorare in continuo il flusso di Hg (massaHg/tempo) lungo il Paglia
2) Limitare erosione sponde
3) Evitare incendi

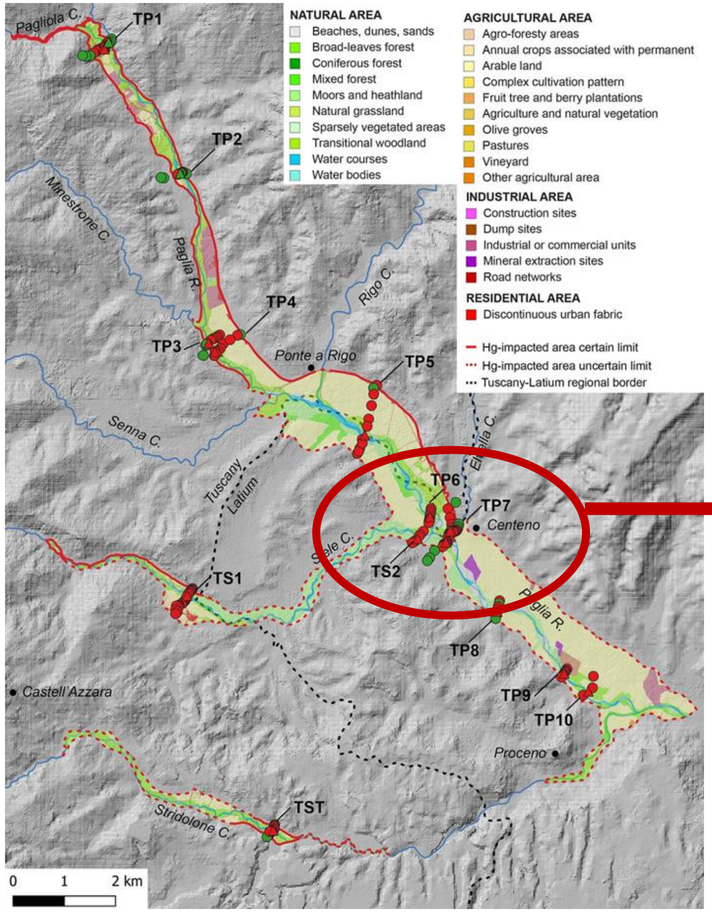

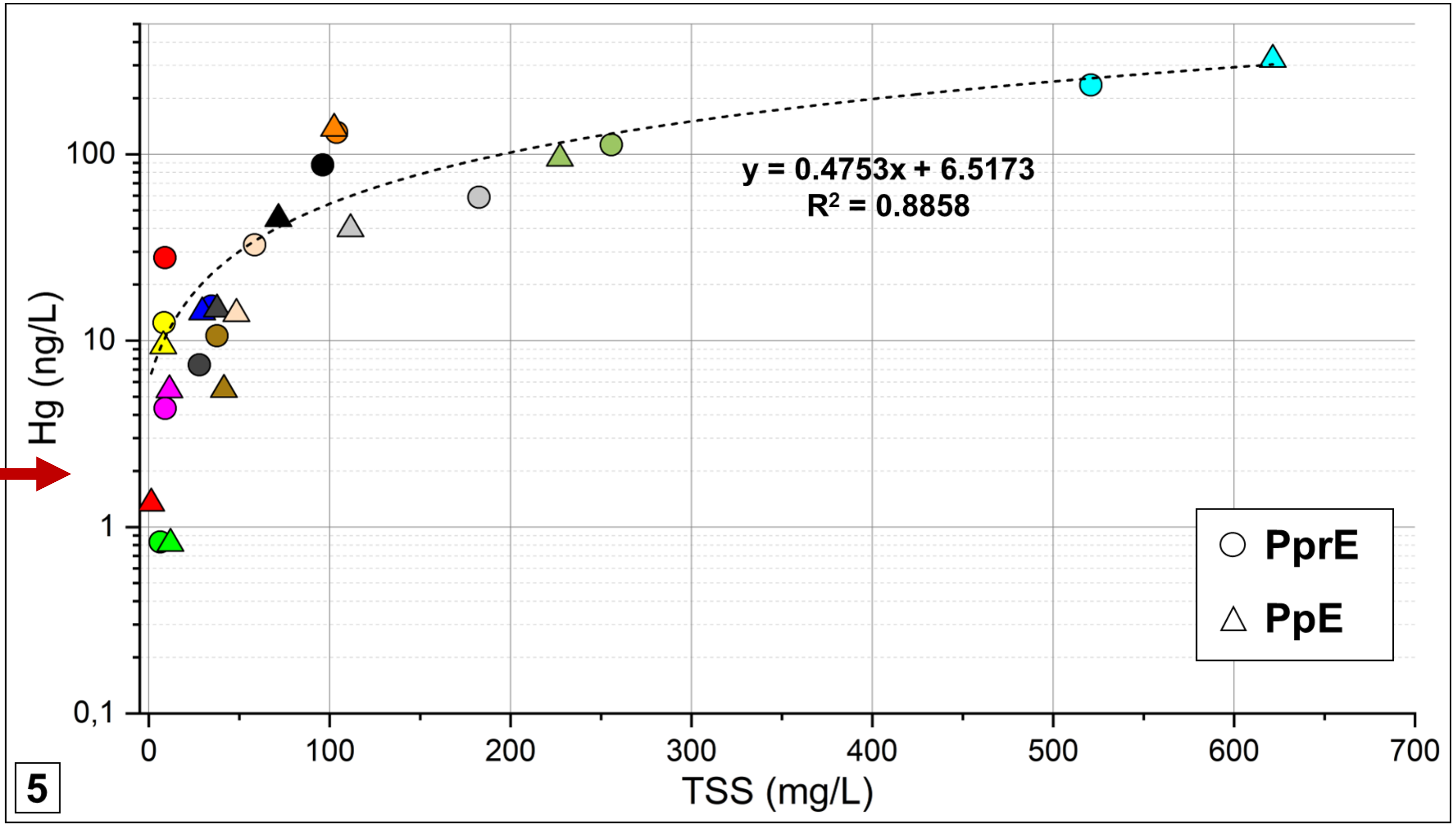

TSS – Hg_p semi-logarithmic plot of the data collected between 2022 and 2023. Sample labels: PprE = Paglia River pre-ECC; PpE = Paglia River post-ECC.

Conclusioni

Growth in mineral needs for low-carbon energy technology

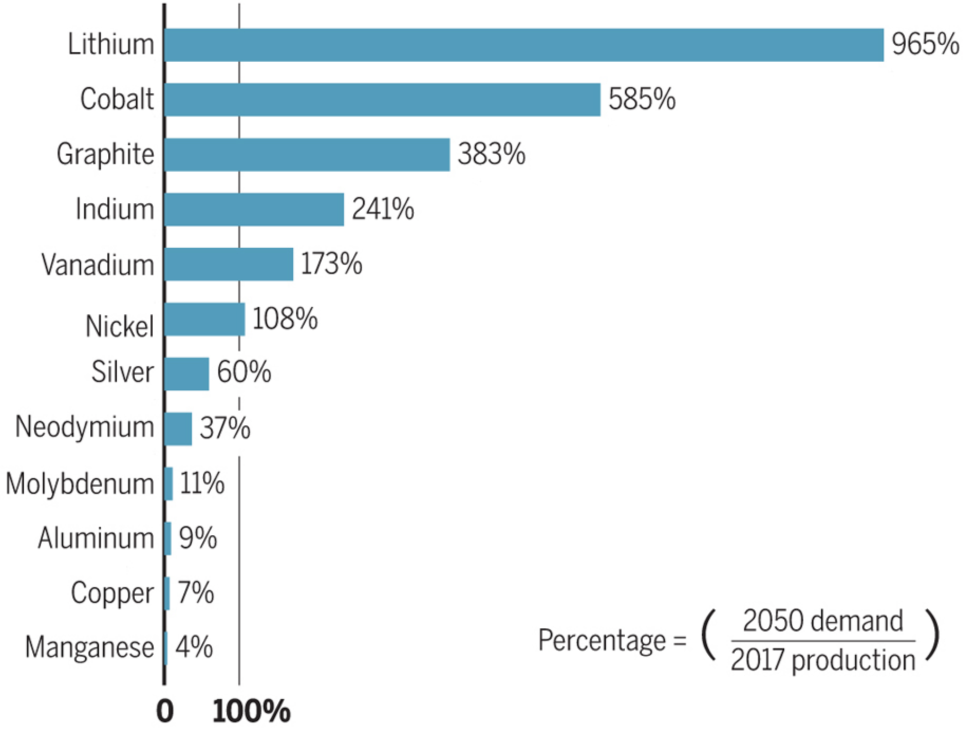

Mineral	Production (kilo–metric tons) 2017	Demand (kilo–metric tons) 2050
Lithium	43	415
Cobalt	110	644
Graphite	1200	4590
Indium	0.72	1.73
Vanadium	80	138
Nickel	2100	2268
Silver	25	15
Neodymium	23	8.4
Molybdenum	290	33
Aluminum	60,000	5583
Copper	19,700	1378
Manganese	16,000	694

All production and demand data reflect annual values. 2017 data reflect annual production for all uses. 2050 data reflect estimated demand for only low-carbon energy technology uses. Data from (*7*).

Science

Sustainable minerals and metals for a low-carbon future

Benjamin K. Sovacool, Saleem H. Ali, Morgan Bazilian, Ben Radley, Benoit Nemery, Julia Okatz, and Dustin Mulvaney

Science **367** (6473), . DOI: 10.1126/science.aaz6003

Vegetazione ripariale

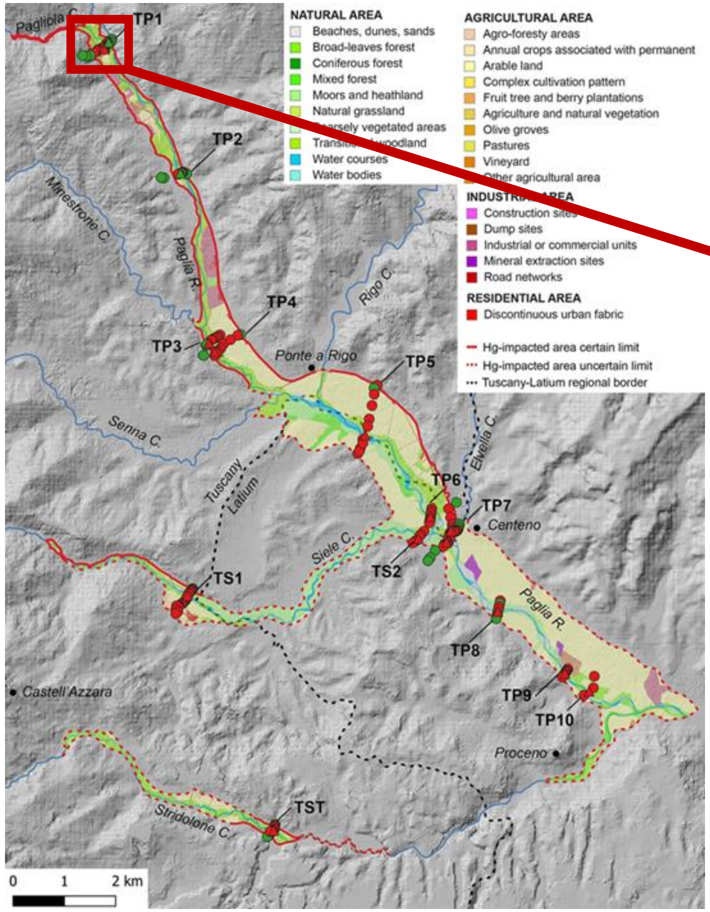

Hg (μg/kg) in tronchi di albero lungo il fiume Paglia: DST ArpaT